

PET/PEN blends of industrial interest as barrier materials. Part I. Many-scale molecular modeling of PET/PEN blends

Maurizio Fermeglia^{a,*}, Paolo Cosoli^a, Marco Ferrone^a, Stefano Piccarolo^b,
Giuseppe Mensitieri^c, Sabrina Pricl^a

^a *Molecular Simulation Engineering (MOSE) Laboratory, Department of Chemical, Environmental and Raw Materials Engineering, University of Trieste, Piazzale Europa 1, 34127 Trieste, Italy*

^b *Department of Chemical, Process and Material Engineering, University of Palermo, Viale delle Scienze, 90128 Palermo, Italy*

^c *Department of Material and Production Engineering, University of Naples Federico II, Piazzale Tecchio 80, 80125 Naples, Italy*

Received 26 March 2006; received in revised form 29 May 2006; accepted 30 May 2006

Available online 23 June 2006

Abstract

Mesoscale molecular simulations, based on parameters obtained through atomistic molecular dynamics and Monte Carlo calculations, have been used for modeling and predicting the behavior of PET/PEN blends. Different simulations have been performed in order to study and compare pure homopolymer blends with blends characterized by the presence of PET/PEN block copolymers acting as compatibilizer. A many-scale molecular modeling strategy was devised to evaluate PET/PEN blend characteristics, simulate phase segregation in pure PET/PEN blends, and demonstrate the improvement of miscibility due to the presence of the transesterification reaction products. The behavior of distribution densities and order parameters of the compatibilized blends demonstrates that mixing properties improve significantly, in agreement with experimental evidences. Barrier properties such as oxygen diffusivity and permeability have also been evaluated by finite element simulations. Accordingly, many-scale modeling seems to be a successful way to estimate PET/PEN blend properties and behavior upon different concentrations and processing conditions.

© 2006 Elsevier Ltd. All rights reserved.

Keywords: PET/PEN blends; Many-scale molecular modeling; Transesterification reaction

1. Introduction

Properties of poly(ethylene terephthalate) (PET)/poly(ethylene 2,6-naphthalate) (PEN) blends have been widely investigated in this decade, due to the enhanced mechanical, thermal and barrier properties (especially in food packaging and preservation) conferred to these mixtures by the presence of a small amount of PEN polymer [1–9]. PET and PEN homopolymers, however, are known to be essentially immiscible at any temperature and composition [10–14]. Nonetheless, miscibility near and above melting temperature is increased as a transesterification reaction takes place, resulting in the formation of PET and PEN copolymers that act as compatibilizer between the PET and PEN phases [11–13,15–18].

Many factors have been found to influence the kinetics of the transesterification reaction, including temperature, annealing time, catalytic system, blend starting composition, viscosity ratio of the two homopolymers, and PET/PEN terminal hydroxyl group capping [5,11,12,19–26]. Yet, as the extent of the transesterification reaction increases, basically two phenomena take place: in the early stages, more and longer block copolymers are formed, further improving blend miscibility, whilst, at later times, the PET and PEN sequence lengths of the existing PET/PEN block copolymer begin to decrease, yielding copolymers of a more random nature [27]. Finally, past some critical level of the so-called degree of randomness (DR) of the forming copolymers, the blend properties become constant, being only a function of the initial blend composition [28]. Eventually, when DR = 1 (i.e., at 100% reaction level), the blend becomes equivalent to a statistical random copolymer as synthesized by melt polymerization. Recently, it has

* Corresponding author. Tel.: +39 040 5583438; fax: +39 040 569823.

E-mail address: mauf@dicamp.units.it (M. Fermeglia).

been demonstrated that an extent of the transesterification reaction of at least 10% is required for a miscible PET/PEN blend; this condition should be granted by a longer annealing time, or by multiple extrusion cycles [26,28].

Material molecular modeling tools have become increasingly integrated in the R&D portfolio. The unique insights available through simulation of materials at a range of scales, from the quantum and molecular, via the mesoscale, to the finite element level, can produce a wealth of knowledge, significantly reduce wasted experiments, allow product and processes to be optimized, and permit large numbers of candidate materials to be screened prior to production. Accordingly, in this work we present, for the first time, the results obtained for the application of a many-scale molecular simulation strategy for the characterization of PET/PEN blends at two different compositions (80/20 and 92/8 %wt), and at several different extents of transesterification reaction, ranging from zero (that is, immiscible systems) to the maximum degree of transesterification theoretically achievable (i.e., PEN has been completely included in the block copolymer). In a forthcoming companion paper (Part II, in preparation), results obtained via many-scale molecular modeling approach will be compared with experimental results on oxygen and carbon dioxide transport in PET/PEN blend and copolymer.

The proposed computational procedure is based on the following ansatz: data obtained from atomistic molecular dynamics (MD) and Monte Carlo (MC) simulations have been used to derive accurate input parameters for mesoscale simulations (MS), and the subsequent use of finite element modeling (FEM), to provide quantitative information regarding the properties of the simulated mesoscale morphologies. In mesoscale modeling, the familiar atomistic description of the molecules is coarse grained, leading to beads of material (representing the collective degree of freedom of many atoms). These beads interact through pair-potentials which capture the underlying interactions of the constituent atoms. The primary output of mesoscale modeling is phase morphologies with size up to the micron level. These morphologies are of interest *per se*, although little prediction of the material properties is available with the mesoscale tools. Finite element modeling then comes into play, and the material properties of interest can be calculated accordingly by mapping the material structures formed at the nanometer scale onto the finite element grid and coupling this information with the properties of the pure components that comprise the complex system. Using standard solvers the finite element code can then calculate the properties of the realistic structured material.

2. Simulation methods and computational details

The main characteristics of the systems considered in this work are summarized in Table 1. The selected simulation temperature was chosen according to the extrusion process thermal conditions reported in Ref. [25], while 18,000 g/mol is a typical value for the molecular weight of industrially employed PET and PEN polymers. Although in some cases low shear rates can be applied during extrusion, at first approximation PET/

Table 1
Characteristics of the simulated PET/PEN blend systems

Simulation	<i>T</i> (K)	PET/PEN copolymer (%wt)	PET <i>M_w</i> (g/mol)	PEN <i>M_w</i> (g/mol)	Blend composition (PET/PEN, %wt)
Set 1	583	0, 8, 15, 30, 40	18,000	18,000	80/20
Set 2	583	0, 8, 15	18,000	18,000	92/08

PEN systems can be modeled in the absence of shear [25]. In the event of a complete transesterification reaction, the calculation of the corresponding degree of randomness, and the estimation of the PET/PEN sequence length in the copolymer have been taken from previous works [6,19]. Further, in these simulations the content of the hetero sequence in the whole blend is about 40%, as all PEN monomers ideally migrate from the PEN homopolymer into the copolymer.

In the many-scale simulation framework adopted, the input parameters for higher scale simulations (e.g., MS) are obtained by performing calculations at lower scales (e.g., MD and MC). All simulations were carried out on an Intel bi-processor XEON 32 bit workstation, using the software modules Amorphous Builder, Discover, and MesoDyn [29–32] as implemented in the commercial platform Materials Studio (v. 3.1, Accelrys, San Diego, CA, USA), and in-house developed software. The Compass forcefield (FF) [33] was used in all MD calculations. The Compass FF is an augmented version of the CFF series of force fields [34,35], and is the first *ab initio* forcefield that has been parameterized and validated using condensed-phase properties in addition to various *ab initio* and empirical data for molecules in isolation. The bond terms of the Compass FF potential energy function include a quartic polynomial both for bond stretching and bending, a three-term Fourier expansion for torsion, and a Wilson out-of-plane coordinate term. Six cross-terms up through 3rd order are present to account for coupling between the intramolecular coordinates. The final two nonbonded terms represent the intermolecular electrostatic energy and the van der Waals interactions, respectively; the latter employs an inverse 9th power term for the repulsive part rather than a customary 12th power term.

The first, key parameter of the MS calculations — the Flory–Huggins interaction parameter χ — was obtained for each system via the solubility parameter δ of the polymers, following the procedure described in detail by Fermeglia and Pricl [36,37], and based on the derivation of the cohesive energy density e_{coh} through MD simulations. Accordingly, each polymer constitutive repeating unit (CRU) with explicit hydrogens was polymerized to the corresponding M_w , and six different amorphous structures for each species were generated by coupling the method originally proposed by Theodorou and Suter [38], based on the rotational isomeric state (RIS) algorithm [39,40] and corrected for incorporation of long-range interactions, with the “scanning method” of Meirovitch [41]. Accordingly, an amorphous phase of a glassy polymer is created in two stages. The conformations of the chains are assumed to resemble those of the unperturbed (from excluded volume interactions) chains that are found with significant probability in the bulk. Thus, initially, a proposed structure can be generated by using

the RIS theory that described the conformations of the unperturbed chains. To avoid excessive overlaps between the chains, modified conditional probabilities are used to account for the nonbonded interactions between the atom to be placed and the rest of the system. Subsequently, the initial structures are minimized by turning on, progressively, the potential energy interactions in a manner such that the more severe overlaps are relaxed first (atomic radii of half the actual size and no-rotational barriers) and, gradually, the minimum is reached by switching on the full potential (radii of actual size, rotational barriers, and attractive interactions). In the scanning method, all possible continuations of the growing chain are taken into account in the calculation of the conditional probabilities. This hybrid scheme method has proved to yield good initial guesses that do not depart much from the random coil hypothesis, have a rather uniform spatial chain segment distribution, and are of relatively low energy. For each polymeric (or copolymeric) system, 10 chains were packed in a cubic simulation box with three-dimensional periodicity. Where available, the initial density of each cell was set equal to the corresponding literature value, in order to minimize discrepancies in the final density values obtained from MD simulations [42,43]. To avoid the system trapping in metastable local high-energy minima, the relaxed structures were subjected to a combined molecular mechanics/molecular dynamics simulated annealing (MDSA) protocol [44–46]: accordingly, the simulation cells underwent five repeated temperature cycles (from 583 K to 1000 K, and from 298 K to 1000 K, and back) using constant volume/constant temperature (NVT) MD conditions. At the end of each annealing cycle, the structures were again minimized via FF, and only those structures corresponding to the minimum energy were used for further modeling. From the fully relaxed models, isothermal–isobaric (NPT) MD experiments were run at 583 K for all systems, and at 298 K for the PET and PEN pure homopolymers. Temperature was controlled via weak coupling to a temperature bath [47], whereas pressure was maintained by coupling to a pressure bath [48]. For the calculation of non-bonded interactions, the cell multipole method [49–51] was employed. This recently developed method is very efficient when dealing with simulation of big systems, as it scales linearly with the number of atoms N , and requires modest memory. Basically, the periodic box is divided into M cubic cells (with $M \approx N/4$ as the optimum choice [51]). For each cell, the cells in the nearest neighborhood contribute to the near-field potentials, and the others to the far-field potential (short- and long-range interactions, respectively). The potential describing each cell has a general form that applies to both Coulombic and London dispersion interactions. The interactions between atoms in the near-field cells are calculated directly for each pair of atoms. For the atom in the far-field cells, the interactions are computed via expansions of multipole moments (charges, dipoles, quadrupoles, and octupoles) around the center of each cell. In this work, a second-order multipole expansion (charges and dipoles) was used, which gives enough accuracy with low overhead. The Newton equation of motions of the 100 ps MD equilibration phase, and of the following 500 ps MD production phase was integrated by the Verlet leapfrog algorithm

[52], using an integration step of 1 fs. The calculations at 298 K were performed with the purpose of testing the selected intermolecular potential/simulation protocol by comparing the theoretically predicted and literature available solubility parameter values.

Now, in general, e_{coh} is defined as the ratio of the cohesive energy E_{coh} and the molar volume V at a given temperature; E_{coh} is in turn defined as the increase in internal energy per mole of substance if all intermolecular forces are eliminated. In our simulated systems, other chains that are simply the displaced images of the chains themselves surround the polymer chains. E_{coh} is the interaction energy between these images. Accordingly, the values of E_{coh} at different temperatures can be obtained from simulation by calculating the difference between the nonbonded energy of the periodic structure, $E_{\text{nb}}^{\text{periodic}}$, and the corresponding value for an isolated parent chain in vacuum $E_{\text{nb}}^{\text{isolated}}$:

$$E_{\text{coh}} = E_{\text{nb}}^{\text{isolated}} - E_{\text{nb}}^{\text{periodic}} \quad (1)$$

For this purpose, 10 parent chains for each polymer (copolymer) were generated, and their energy was minimized according to the procedure described above. The MDSA protocol was again applied to provide thermal energies to cross energy barriers between conformation local minima. NVT MD simulations were then performed on the single chains (again the 10 best relaxed chains for each system) in vacuum at the same temperature conditions applied to the simulation of the relevant periodic systems. The appropriate δ values were thus obtained as:

$$\delta = \sqrt{e_{\text{coh}}} = \sqrt{E_{\text{coh}}/V} \quad (2)$$

The corresponding Flory–Huggins parameters were estimated as:

$$\chi_{1,2} = \frac{(\delta_1 - \delta_2)^2}{RT} V_{1,2} \quad (3)$$

where $V_{1,2}$ was considered as the average molecular volume of the different CRUs present in the system, weighted over the corresponding volume fractions.

The theory underlying the methodology for the calculations of the next set of MS input parameters – the number N_{meso} and the bond length a of the MS beads – is similar to the classical dynamic random phase approximation (RPA) [53,54]. The polymer chains are modeled as Gaussian chains consisting of beads, each bead representing a number of monomers of the real polymer. The mapping of the real polymer chains onto Gaussian chains can be obtained via the characteristic ratio C_∞ , by imposing the mean-square end-to-end distance, and the length of the freely jointed chain to be equal for the real and the Gaussian chain. Thus, we have:

$$C_\infty = \lim_{n \rightarrow \infty} \frac{\langle r^2 \rangle_0}{\sum_i n_i l_i^2} \quad (4)$$

in which $\langle r^2 \rangle_0$ denotes the mean-square end-to-end distance of an unperturbed chain molecule in solution, n is the number of

bonds along the shortest path across the backbone, and n_i is the number of times the j th bond which has a length of l_i , occurs along this shortest path. If we consider the real chain to be constituted by N monomers of length l , then it can be approximated by a freely jointed equivalent chain characterized by a smaller number of segments, N_{meso} , each with a higher bond length a . The choice of n and a must, therefore, comply with the following two conditions: the first is given by Eq. (4), so that:

$$\langle r^2 \rangle_0 = C_\infty N l^2 = N_{\text{meso}} \bar{a}^2 \quad (5)$$

whilst the second condition sets that:

$$N_{\text{meso}} a = l_{\text{max}} \quad (6)$$

where a is the modulus of the bond vector \bar{a} , and l_{max} is the length of the fully extended chain, given in turn by:

$$l_{\text{max}} = N l \sin \frac{\theta}{2} \quad (7)$$

Substituting Eq. (7) in Eq. (6), and dividing Eq. (5) by Eq. (6), we finally get the relevant expressions for the mesoscale input parameters N_{meso} and a :

$$a = \frac{C_\infty l}{\sin \frac{\theta}{2}} \quad (8)$$

$$N_{\text{meso}} = \frac{N}{C_\infty} \sin^2 \frac{\theta}{2} \quad (9)$$

Generally speaking, the best-known method for calculating the conformational properties of polymer chains is the RIS theory described above. However, there are some technical difficulties preventing the routine and straightforward application of RIS in a reliable manner to polymers with complex CRU structures, and especially to polymers containing rings along their backbone. For this purpose, a new method, called RIS Metropolis Monte Carlo (RMMC) was recently proposed by Honeycutt [55]. The first stage of an RMMC calculation consists of the optimization of the geometry of the starting model chain by energy minimization. The second stage consists of a Monte Carlo simulation of the conformational degrees of freedom, to calculate the properties of interest. Only the torsional degrees of freedom are allowed to vary at this stage. The effects of the torsional motions possible around the rotatable bonds along the chain backbone are explored by a sequence of steps which are attempted, and accepted or rejected, by conventional Monte Carlo simulation techniques. The torsional degrees of freedom of side groups can also be considered during an RMMC calculation. However, since this option is mainly useful when model chains contain large or highly flexible side groups, we did not include them in our calculations. The MC simulation is also performed in two stages. The first consists in equilibrating the starting chain by using a large number of MC steps. An even larger number of steps are employed in the following production

stage. The polymer conformational properties are then averaged over the entire production stage, so that both the average value and the relevant error values are estimated for each property. A limitation of the RMMC is that a polymer chain consisting of very rigid subunits linked in an entirely collinear manner (e.g., poly(*p*-phenylene)), would be predicted to remain a true rigid rod during the entire simulation, leading, for instance, to an infinite value of C_∞ . In reality, the C_∞ value of such a polymer is large but remains finite, since bond angle distortions can cause “buckling” motions which change the chain end-to-end distance, even in totally linear rigid rod macromolecules, whose torsional motions do not change the end-to-end distance [56,57]. However, since the torsional motion changed the chain end-to-end distance by significant amounts in the PET/PEN polymers of interest, this limitation was not considered as a serious concern in our case.

From an operative standpoint, starting from the minimized polymer chains generated to be employed in the MD simulations, 200,000 MC steps were used in the equilibration stage, and 1,000,000 steps constituted the production portion of the MC simulation. Again, two calculation sets were performed: at $T = 583$ K and $T = 298$ K, for comparison with available literature data. The maximum number of rotatable backbone bonds separating two atoms, at which the nonbonded interactions are still included in the energy calculation during the MC simulation was set to 8.

The core of this work is, however, the use of mesoscale simulations with MesoDyn [29–32]. As said, the starting point for an MS simulation is a coarse grained model for the diffusive and hydrodynamic phenomena in phase separation dynamics [32]. The thermodynamic forces are obtained via a mean-field density functional theory, assuming a Gaussian chain as a molecular model. The melt dynamics are described by a set of stochastic partial differential equations (functional Langevin equations) for polymer diffusion. Noise sources, with correlations dictated by the fluctuation–dissipation theorem, introduce the thermal fluctuations. The numerical calculations involve the time-integration of functional Langevin equations, given an implicit Gaussian density functional expression for the intrinsic chemical potentials.

Since the theory at the base of MesoDyn is extensively described in the papers from the Fraaije group, we will summarize it here only briefly. The model used in the MesoDyn project consists of beads of various types I, J, \dots with interactions described by harmonic oscillator potentials for the intramolecular interactions in the Gaussian chain (ideal interactions), $F^{\text{id}}[\rho]$, whilst the intermolecular interactions between the chains (nonideal interactions) are introduced by a mean-field potential F^{nid} of the form:

$$F^{\text{nid}}[\rho] = \frac{1}{2} \sum_{I,J} \int \int \epsilon_{IJ}(|\mathbf{r} - \mathbf{r}'|) \rho_I(\mathbf{r}) \rho_J(\mathbf{r}') d\mathbf{r} d\mathbf{r}' \quad (10)$$

in which $\rho_I(\mathbf{r})$ is the density of bead type I at \mathbf{r} (local bead concentration), and $\epsilon_{IJ}(\mathbf{r} - \mathbf{r}')$ is a cohesive interaction

between beads I at \mathbf{r} and J at \mathbf{r}' , chosen to have a Gaussian form:

$$\epsilon_{IJ}(|\mathbf{r} - \mathbf{r}'|) = \epsilon_{IJ}^0 \left(\frac{3}{2\pi a^2} \right)^{3/2} e^{-(3/2a^2)(\mathbf{r} - \mathbf{r}')^2} \quad (11)$$

In Eq. (11), a is the Gaussian bond length, and ϵ_{IJ}^0 is the constant cohesive interaction between beads I and J which can be taken equal to the Flory–Huggins parameter χ .

The total free energy is then defined as:

$$F[\rho] = F^{\text{id}}[\rho] + F^{\text{mid}}[\rho] \quad (12)$$

If additional external potentials $U_I(\mathbf{r})$ are coupled to the Hamiltonian of the system in order to constrain the density fields $\rho_I(\mathbf{r})$ to the observed densities $\rho_I^0(\mathbf{r})$, then the corresponding free energy functional can be defined as:

$$F[\psi] = \text{Tr}(\psi H^{\text{id}} + \beta^{-1} \psi \ln \psi) + \sum_I \int_V U_I(\mathbf{r}) [\rho_I[\psi](\mathbf{r}) - \rho_I^0(\mathbf{r})] d\mathbf{r} + F^{\text{mid}}[\rho^0] + \lambda [\text{Tr} \psi - 1] \quad (13)$$

in which ψ is the configurational distribution, that is, the distribution of the bead positions, H^{id} is the Hamiltonian of the Gaussian chain, and $\beta^{-1} \psi \ln \psi$ is the entropy of the distribution. Tr is defined as:

$$\frac{1}{n! \mathcal{A}^{3nN}} \int d\mathbf{r}_{11} \dots d\mathbf{r}_{nN} \quad (14)$$

where \mathcal{A} is the de Broglie thermal wavelength, n the number of chains, and N the number of beads per chain. The last term in Eq. (13) normalizes the distribution ψ , λ being a Lagrange multiplier. Accordingly, the minimization of $F[\psi]$ with respect to ψ leads to a distribution that is determined by the external potential $U_I(\mathbf{r})$. At every simulation time step, the distribution ψ is the one that minimizes the free energy, and constrains the density fields $\rho_I(\mathbf{r})$. These, in turn, are determined by ψ . This results in the bijectivity concept (that is, a one-to-one relation between the external potentials and the density fields) which is fundamental for the method.

The dynamics of the model are described by the following set of diffusion equations (generalized time-dependent Ginzburg–Landau model):

$$\frac{\partial \rho_I(\mathbf{r}, t)}{\partial t} = \sum_{j=1}^N \int D_{IJ}(\mathbf{r}, \mathbf{r}', t) \frac{\delta F}{\delta \rho_j}(\mathbf{r}', t) d\mathbf{r}' + \eta_I(\mathbf{r}, t) \quad (15)$$

with the diffusion operator D_{IJ} , and noise η_I , with correlations given by:

$$\langle \eta_I(\mathbf{r}, t) \rangle = 0 \quad (16)$$

$$\langle \eta_I(\mathbf{r}, t) \eta_J(\mathbf{r}', t') \rangle = -2\beta^{-1} D_{IJ}(\mathbf{r}, \mathbf{r}', t) \delta(t - t') \quad (17)$$

The set of diffusion equations is closed by the expression for the free energy:

$$\frac{\delta F}{\delta \rho_I} = -U_I(\mathbf{r}) + \frac{\delta F^{\text{mid}}}{\delta \rho_I} \quad (18)$$

If a local coupling approximation is used, the diffusion operator is given by:

$$D_{IJ}(\mathbf{r}, \mathbf{r}') = \beta D \delta_{IJ} \delta(\mathbf{r} - \mathbf{r}') \nabla_{\mathbf{r}} \cdot \rho_J(\mathbf{r}) \nabla_{\mathbf{r}'} \quad (19)$$

with diffusion constant D .

A typical MS simulation was then performed using the required input parameters, obtained via the atomistic simulation approach outlined above, and with following operative settings for the integration of the dynamic equations: cell dimension = 73.8 nm, grid dimensions = $32 \times 32 \times 32$, grid spacing = 2.305 nm, noise factor = 75, time step = 50 ns, number of steps = 15,000, maximum number of iterations per step = 100.

Finally, the density distributions obtained from mesoscale simulations have been used as input data for finite element calculations with the MesoProp software [58,59]. MesoProp uses a numerical method to determine the overall properties of composites with arbitrary morphologies from the properties of the components based on small homogeneous grid elements. Morphologies are defined by a number of phases in a periodically continued base cell of cubic or orthorhombic shape, where the resolution depends on the number of grid elements used. To avoid boundary effects in the simulation of the material properties, three dimension periodic boundary conditions are used in the simulation. By applying a displacement-based finite element method to the volume mesh, the responses to external deformations are calculated [59]. The solver works on the basis of a space-filling tetrahedral mesh, i.e. without voids. The mapping of cubic grid elements to a tetrahedral mesh results in six isochoric tetrahedrons for each cubic grid element. The number of mesh elements is six times the number of grid nodes, which is equal to the number of grid elements. For transport properties, a Laplace solver is used that applies a field in the three main directions to the finite element mesh, and minimizes the energy of the composite.

In our case, grid morphologies were obtained for all systems studied by importing the corresponding density distributions from the relevant MS simulations. Density, diffusivity and permeability values for oxygen in pure, amorphous homopolymers have been taken from the literature [60]. To a first approximation, the degree of crystallinity of the polymers was taken into consideration by assuming the van Krevelen relationships [61] for gas diffusivity D and solubility S :

$$D_{\text{SC}} = D_{\text{G}}(1 - X) \quad (20)$$

$$S_{\text{SC}} = S_{\text{G}}(1 - X) \quad (21)$$

where D_{SC} and S_{SC} are the diffusivity and solubility of semi-crystalline homopolymers characterized by a degree of crystallinity equal to X , respectively, and D_{G} and S_{G} are the diffusivity and solubility values for the corresponding pure amorphous chains. The well-known relation between S and D , $P = S \times D$, coupled to Eqs. (20) and (21), finally yields the corresponding expression of the permeability of semi-crystalline systems as:

$$P_{\text{SC}} = S_{\text{G}} D_{\text{G}} (1 - X)^2 \quad (22)$$

3. Results and discussion

3.1. Validation of atomistic simulations and input parameter sets for mesoscale simulations

As a first step, the correctness of the atomistic simulation strategy employed to calculate the input parameters for MS simulations of the systems under consideration was examined. For this purpose, the values of the solubility parameter δ and the density ρ , obtained from MD simulations, and the characteristic ratios C_∞ , calculated from MC simulations, are shown in Table 2, along with literature data for comparison [60–63]. As can be seen from this table, the agreement between simulated and literature values is excellent; accordingly, these evidences can be taken as a validation of the computational procedure adopted to calculate these molecular parameters.

The entire set of MS input parameters obtained from lower scale molecular simulations is listed in Table 3. It should be noticed that bead self-diffusion coefficient D was appropriately set to 2×10^{-7} cm²/s to avoid the simulation dimensionless time step τ (i.e., the product of the time step and the bead diffusion coefficient, divided by the square of the grid spacing) to exceed the recommended limit [29–32]. It has been seen, however, that the self-diffusion parameter does not have an appreciable effect on the final structure of the MesoDyn simulation (data not shown). The compressibility parameter K was left at its default value of 10.

3.2. MS simulations of PET/PEN blends without transesterification

As the first case, PET/PEN homopolymer blends' miscibility in the absence of transesterification reaction has been examined. In agreement with the corresponding experimental evidences [10–14], these systems show a complete phase segregation at the processing temperature considered (583 K), as shown by the three-dimensional bead volumetric density distribution reported in Fig. 1a. From this figure we can infer that a little amount of immiscible PEN homopolymers will slowly find a way for aggregation in separated clusters. Moreover, it can be seen that the smaller the quantity of species, the longer the pathway they have to travel to ensemble into aggregates.

Due to the low PEN concentration in the 80% PET/20% PEN blend, the system shows a slow convergence towards a free energy stable condition. This can be evaluated by

Table 2

Solubility parameters δ , densities ρ , and characteristic ratios C_∞ for PET and PEN homopolymers obtained from atomistic MD and MC simulations at 298 K

	δ_{sim} (MPa ^{1/2})	δ_{lit} (MPa ^{1/2})	$C_{\infty, \text{sim}}$ (–)	$C_{\infty, \text{lit}}$ (–)	ρ_{sim} (g/cm ³)	ρ_{lit} (g/cm ³)
PET	21.9	19.9–21.9	4.02	4.11	1.329 ± 0.003	1.336
PEN	18.1	–	5.27	5.33	1.334 ± 0.004	1.327

The 2nd, 4th and 6th columns list the corresponding literature data, for comparison.

Table 3

MS input parameter set for PET/PEN systems

	C_∞ (–)	δ (MPa ^{1/2})	D (cm ² /s)	K (m ² kg s ⁻²)	χ (–)	N_{meso} (–)	a (nm)
PET	4.02	21.9	2×10^{-7}	10	0.523	23	2.661
PEN	5.27	18.1	2×10^{-7}	10	0.523	14	2.661

controlling the so-called order parameter P_I , defined for each species I as the deviation from the mean bead density at homogeneity:

$$P_I = \frac{1}{V} \int_V [\theta_I^2(\mathbf{r}) - \theta_{I,0}^2] d\mathbf{r} \quad (23)$$

where θ is a dimensionless density (volume fraction) for bead species I , and the index 0 denotes average values at homogeneity. According to Eq. (23), order parameters with large values indicate strong phase segregation. Conversely, very small values of P_I correspond to homogeneous systems. The

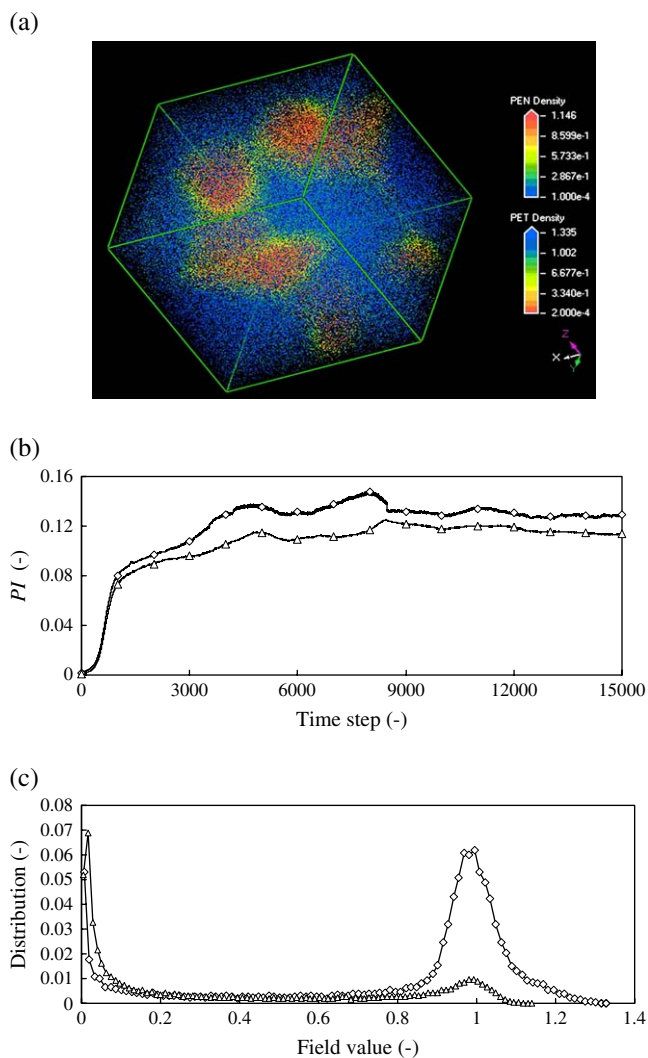


Fig. 1. Three-dimensional bead volumetric density distribution (a), order parameter P_I (b) and density field distribution (c) of the phase segregation for the 80% PET/20% PEN blend system at 583 K and in the absence of transesterification reaction. Symbols: \diamond , PET; \triangle , PEN.

behavior of P_I for this PET/PEN system is illustrated in Fig. 1b, from which both the long times involved in system free energy equilibration and high final values of the P_I parameter are quite evident. Lastly, Fig. 1c reports the density field distribution of the PET and PEN species. It should be noticed that probability densities of PET and PEN have two small peaks at different bead densities, which are a clear indication that segregation occurs: PET and PEN are both present at densities close to 0 and close to 1.

Utterly analogous results were obtained for the blend characterized by a lower amount of PEN, i.e., 92% PET/8% PEN.

3.3. MS simulations of PET/PEN blends in the presence of a transesterification reaction

When the transesterification reaction takes place, pure homopolymers are progressively substituted by block copolymers that became more random in nature as long as the reaction proceeds. Patchek and Jabarin [6] proposed the following equations for the estimation of the average sequence lengths of ethylene terephthalate and naphthalate units – L_T and L_N , respectively – in the copolymers:

$$L_T = \frac{1}{(1 - X_T)DR} \quad (24)$$

$$L_N = \frac{1}{(1 - X_N)DR} \quad (25)$$

where X_T and X_N are the molar fractions of PET and PEN, respectively, and DR is the degree of randomness. DR can be defined as the sum of the probabilities of finding a naphthalate unit next to a terephthalate one (P_{tn}), and a terephthalate unit next to a naphthalate one (P_{nt}) [63]. Ihm et al. [13] examined the extent of transesterification in a 50/50 PET/PEN blend as a function of the annealing time: they found that the longer the annealing time, the higher the DR and the shorter the block sequence length into the copolymer. In order to simplify the situation for the MS simulations, we assumed as the first case of study that an ideal, complete transesterification reaction takes place (40 %wt of copolymer in the blend, see Table 1); accordingly, the corresponding block copolymer model structure contains short blocks of each repeating units. The number of beads for each repeating unit in the copolymer was then calculated as:

$$B_{N_i} = \frac{r}{C_\infty} \quad (26)$$

where r is the number of repetitions of each CRU in the blocks, and B_{N_i} is the bead number for each block. For further sake of simplicity, we decided to alternate PET and PEN beads; the copolymer weight was arbitrarily fixed at 36,000 g/mol, which corresponds to ideal condensation of one chain of PET and one of PEN. As previously remarked, all PEN homopolymers have been incorporated into the copolymer. Accordingly, with reference to the MS input parameters reported in Table 3, the number of beads of the molecule types become 23 for

PET, 0 for PEN and 14 + 23 (suitably alternated) for PEN and PET in the copolymer, all other values being equal to those listed in Table 3. We also performed further simulations at intermediate transesterification degrees, both for the 80% PET/20% PEN, and the 92% PET/8% PEN blend systems (see Table 1). Finally, in order to visualize and emphasize the displacement of PET beads in the simulation grid, PET beads in the copolymer were given a different nomenclature (i.e., PETCO), although they are obviously characterized by the same χ parameter of the PET beads in the PET homopolymer.

The results obtained from the MS simulation at complete transesterification clearly differ from the previous case, as can be observed looking at the corresponding three dimension – bead volumetric density distribution (Fig. 2a), the order parameter P_I , and the density field distribution (Fig. 2b and c),

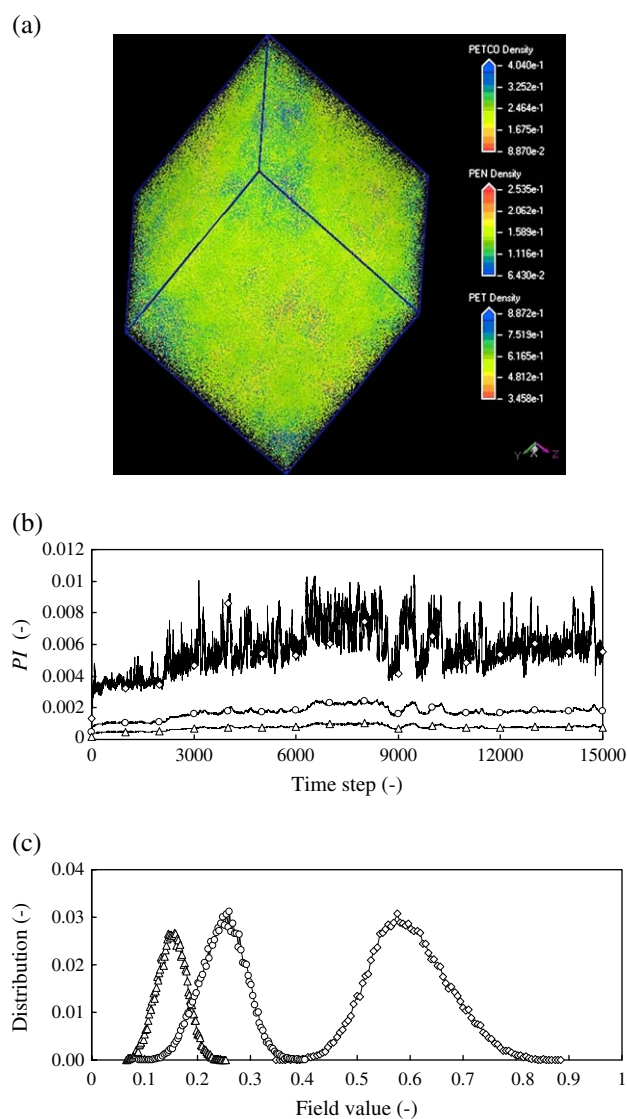


Fig. 2. Three-dimensional bead volumetric density distribution (a), order parameter P_I (b) and density field distribution (c) of the phase segregation for the 80% PET/20% PEN blend system at 583 K and in the presence of complete transesterification reaction. Symbols: \diamond , PET; \triangle , PEN; \circ , PETCO.

respectively. The homogeneity of the system is qualitatively well evidenced by the uniform yellow-green color throughout the cell, corresponding to average bead densities close to their initial values (see Fig. 2a). The equilibrium values of P_I are at least two orders of magnitude lower than the corresponding case without transesterification (see Fig. 2b), and the probability density profiles show a single well-defined peak for each species, further featuring a narrow distribution around the mean initial value (see Fig. 2c).

The sensible, rather obvious explanation for the improved miscibility envisaged in this system can be the compatibilization effect induced by the copolymer, which is able to compensate the repulsion between PET and PEN beads. Short blocks in the copolymer exert a sort of “bridging” effect between the homopolymers, reducing the mean displacement of the beads, and avoiding phase segregation into bigger clusters.

As intermediate situations are more common in nature, further simulations have been performed in order to evaluate the influence of different extent of transesterification. Also, according to the foregoing discussion, the evaluation of miscibility for different degrees of transesterification may reveal some interesting information from an industrial point of view, as the amount of copolymer formed depends upon time, temperature and type of extrusion. According to the literature evidences [13] that report PET and PEN sequence length reduction with transesterification, we evaluated the phase segregation effect upon transesterification assuming that the block copolymers, as previously mentioned, become more random in nature as the transesterification proceeds. This practically corresponds to shorter bead sequences in the copolymer mesoscale architecture.

As the graphs in Fig. 3 clearly show, the order parameters decay almost linearly with increasing extent of the transesterification reaction, that is, as the compatibilizer copolymer becomes progressively more and more random in its primary sequence.

Interpreting density field distributions in a many-phase system to decide whether segregation takes place is not always easy [13]. In some cases segregation occurs when the system shows different glass transition temperatures, T_g ; here, the segmental size responsible for a single T_g is about 100 Å, a dimension almost comparable to the one involved in our simulations (about 74 nm). Such a dimension is, however, smaller than, for example, the limit of the optical range, where the crucial factor is the haziness. In this case, optical clarity can be reached with a lower degree of transesterification, as bigger segregation domains may not exclude homogeneity. Definitely, the response depends upon the size of heterogeneities which defines phase separation.

Table 4

Literature values for oxygen permeability (P_G), diffusion (D_G), solubility (S_G) [60], and degree of crystallinity X for amorphous PET and PEN homopolymers [61], and values of P_{SC} , D_{SC} and S_{SC} for the corresponding semi-crystalline species as calculated via Eqs. (20)–(22)

	P_G (barrer)	D_G (cm ² /s)	S_G (cc(STP)cm ⁻³ atm ⁻¹)	X (-)	P_{SC} (barrer)	D_{SC} (cm ² /s)	S_{SC} (cc(STP)cm ⁻³ atm ⁻¹)
PET	7.05×10^{-2}	5.2×10^{-9}	0.103	0.31	3.35×10^{-2}	3.6×10^{-9}	0.0711
PEN	2.54×10^{-2}	1.6×10^{-9}	0.121	0.43	8.20×10^{-3}	9.1×10^{-10}	0.0690

1 Barrer = 7.5005×10^{-18} m²/s/Pa.

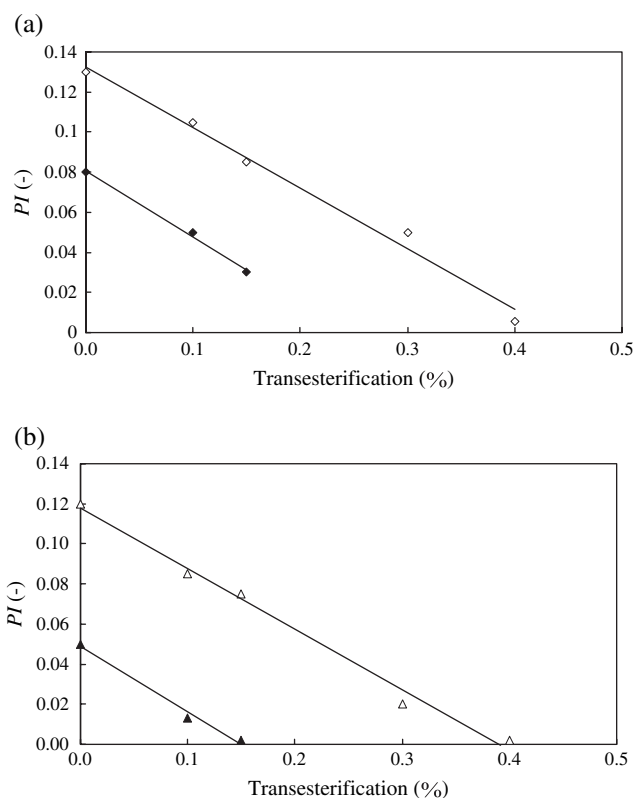


Fig. 3. Order parameter P_I for PET (a) and PEN (b) as function of the extent of the transesterification reaction. Open symbols: blend composition 80% PET/20% PEN; filled symbols: blend composition 92% PET/8% PEN.

3.4. Finite element calculations

In order to evaluate the barrier effects such as permeability and diffusivity of oxygen in the PET/PEN blends, we performed simulations on both 80% PET/20% PEN and 92% PET/8% PEN systems at a finite element level and in the two limit conditions: (i) without transesterification, and (ii) in the presence of a complete transesterification. Importantly, the density distributions obtained from the relevant MS were used as input data for these calculations. As PET and PEN polymers are both endowed with a certain degree of crystallinity, for these simulations we used the literature available values of the degree of crystallinity, P and D , and Eqs. (20)–(22) to obtain the corresponding values of the semi-crystalline homopolymers, as shown in Table 4.

Figs. 4(a) and 5(a) illustrate the O_2 permeability P of the blends along the z axis for the 80% PET/20% PEN system, in the case of no transesterification (Fig. 4a) and with complete transesterification reaction (Fig. 5a), respectively. Figs. 4(b) and 5(b) visualize the corresponding distributions of P

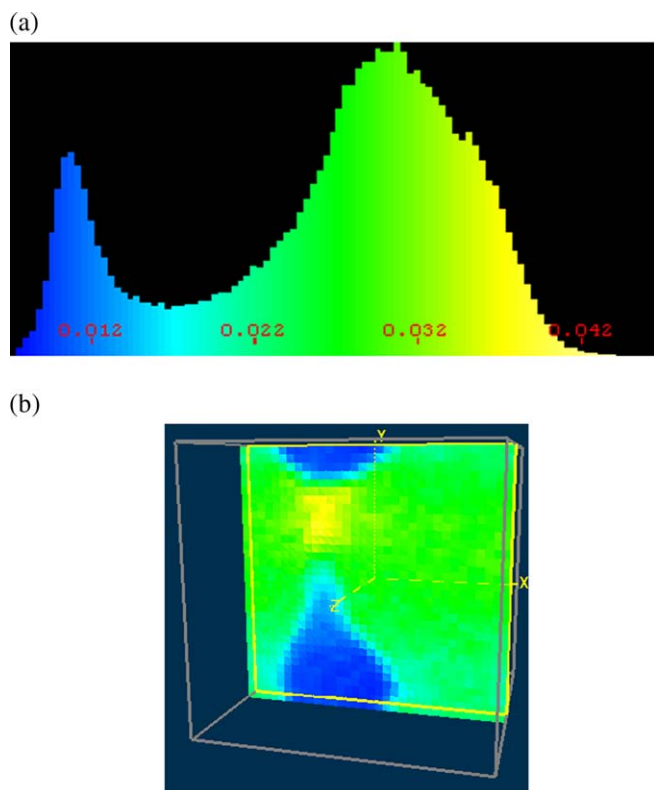


Fig. 4. Oxygen permeability P along the z axis (a) and permeability distribution in the xy plane (b) for the 80% PET/20% PEN system without transesterification.

in the xy plane. Analogous results have been obtained in the x and y directions, and for the diffusivity D (data not shown). The average values for P and D as obtained from the simulations are listed in Table 5.

Blends without transesterification clearly show two peaks (see Fig. 4(a)), due to the presence in the cell of two separated phases with quite different barrier properties. This also justifies the higher standard deviations for P and D in such systems (see Table 5), as these parameters strongly vary in the cell. On the other hand, in miscible blends P and D show only one peak, with lower standard deviations, in harmony with the more homogeneous structural topology. A glance at Table 5 further reveals that barrier properties are only moderately improved by blending PET with PEN, at least up to 20% PEN. The analysis of both permeability and diffusivity suggests that when segregation occurs, the barrier effect increases slightly. This is probably caused by the hindering

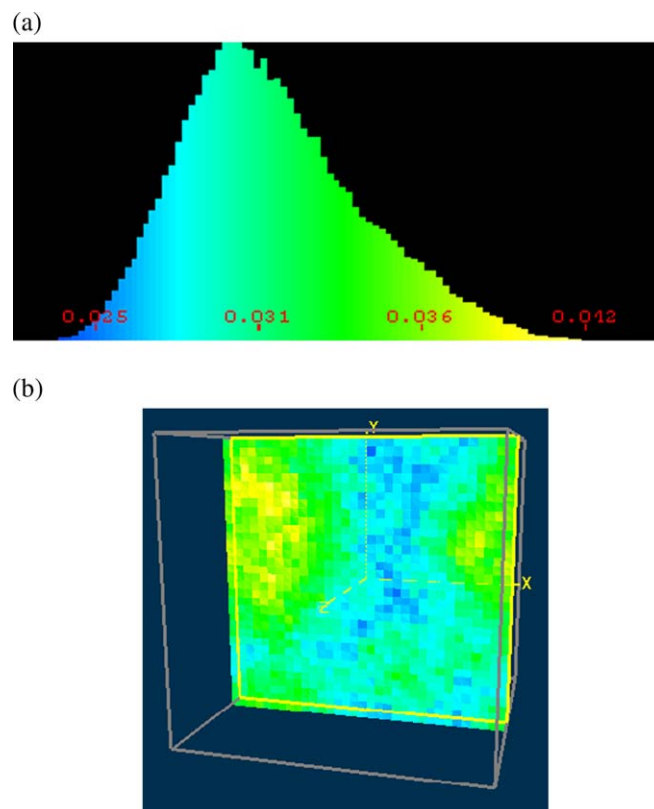


Fig. 5. Oxygen permeability P along the z axis (a) and permeability distribution in the xy plane (b) for the 80% PET/20% PEN system with transesterification.

effect of the larger domains of PEN that partly obstruct the oxygen displacement in the system. This further seems to indicate that in PET/PEN blends barrier effects are enhanced by larger amount of PEN, possibly with a higher degree of crystallization, and preferably with the creation of large domains which are improved when segregation phase occurs.

Fig. 6 summarizes the estimated barrier effect improvement due to the presence of PEN in the case of both 92% PET/8% PEN and 80% PET/20% PEN. As clearly demonstrated, permeability and diffusivity changes are confined, especially if compared, for instance, with industrial food packaging permeability requirements (one or even more order of magnitude less). Fig. 6 shows that an improvement in the barrier effect is obtained for (i) an increasing amount of PEN in the blend at constant degree of transesterification and (ii) a decreasing degree of transesterification at constant composition. The first trend is a consequence of the pure component properties of the

Table 5

Average values for oxygen permeability P and diffusion D in 80% PET/20% PEN systems without transesterification and with complete transesterification

	P (barrer)	D (cm ² /s)
PET	3.35×10^{-2}	3.59×10^{-9}
PEN	8.20×10^{-3}	9.10×10^{-10}
80% PET/20% PEN no transesterification	$2.71 \times 10^{-2} \pm 1.45 \times 10^{-4}$	$2.92 \times 10^{-9} \pm 1.17 \times 10^{-11}$
80% PET/20% PEN complete transesterification	$2.96 \times 10^{-2} \pm 2.80 \times 10^{-6}$	$3.18 \times 10^{-9} \pm 1.21 \times 10^{-12}$
92% PET/8% PEN no transesterification	$3.07 \times 10^{-2} \pm 1.23 \times 10^{-4}$	$3.29 \times 10^{-9} \pm 1.33 \times 10^{-11}$
92% PET/8% PEN complete transesterification	$3.18 \times 10^{-2} \pm 5.57 \times 10^{-5}$	$3.41 \times 10^{-9} \pm 2.80 \times 10^{-12}$

1 Barrer = 7.5005×10^{-18} m²/s/Pa.

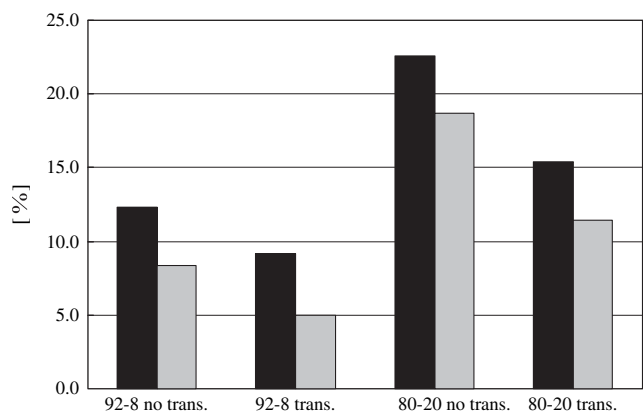


Fig. 6. Comparison of barrier effect improvement (in % with respect to the pure PET) for oxygen permeability (black bars) and diffusivity (grey bars) in semi-crystalline PET/PEN blends as estimated according to the many-scale molecular simulation approach.

two polymers, while the second one indicates that the domains of PEN in the nonhomogeneous PET/PEN blend are responsible for a small enhancement in the barrier effect even in the absence of clusters of crystals.

In any case, the trend for blends with higher PEN percentage seems to exclude the fact that notable barrier properties could be achieved in the PEN concentration range considered. Considering the high market cost of the PEN material, all these evidences may suggest that, when the ultimate goal consists in the achievement of high improvements in barrier properties, alternative routes should be pursued such as, for instance, the design of suitable PET-organoclay nanocomposites.

4. Conclusions

Molecular simulation is a useful tool for studying the microscopic structure and understanding the mechanism of physical processes on molecular/supramolecular levels. In particular, molecular simulations of polymeric structures have reached the stage where they are now helpful in gaining insights into the molecular origins of behavior of bulk polymers. In this paper, we have investigated the phase behavior of PET/PEN blends both in the absence and presence of a transesterification reaction, and calculated some transport properties of oxygen in these blends in the light of possible applications as barrier materials.

According to the multi-scale molecular modeling ansatz proposed in this paper, the input parameters necessary to perform calculations at a higher length scale level (e.g., meso-scale) have been obtained by performing simulations at a lower length scale (e.g., atomistic molecular dynamics and/or Monte Carlo). The procedures have been validated against experimental evidences, showing excellent agreement.

Mesoscale molecular modeling of PET/PEN homopolymer blends has demonstrated complete immiscibility for these systems, in net agreement with literature results provided by previous experimental tests. As a transesterification reaction usually occurs during the extrusion process of these materials, the many-scale simulation approach adopted in this work

demonstrates that miscibility is improved by a longer annealing process or, in other words, by longer transesterification times. In particular, by assuming an ideal situation according to which a complete transesterification is achieved, the system is completely mixed. Differences between the segregated and mixed systems are quite evident, as the relevant order parameters differ by two orders of magnitude, and, in the case of transesterification, probability densities are narrowly distributed around a single value.

Imposing a higher degree of randomness in the copolymer favors miscibility, as at the end of the simulation bead density distribution varies weakly in each grid. The trend that testifies a higher induced miscibility with a deep transesterification has been fully confirmed by mesoscale molecular modeling. Simulations can be helpful to predict the behavior of the blend at different levels of transesterification, temperature and, at the occurrence, shear rate.

Finally, further investigation with finite-difference simulations has been performed to obtain the physical properties of the blends. Barrier effects such as permeability and diffusivity were calculated for miscible and immiscible blends. In the first case, the effects can be summarized by a quasi-Gaussian distribution with one neat peak, while in the second case the creation of large domains due to segregations reflects the presence of two peaks. Globally, however, only a modest increment of the barrier properties in the immiscible blends can be detected, as the creation of larger domains partially hinders the displacement of the gaseous molecules. Therefore, alternative routes such as PET/organoclay nanocomposites could constitute a better and more efficient way to confer higher barrier effect to this polymeric material.

In order to verify these conclusions, based on the innovative computational approach proposed in this paper, an extensive comparison of the modeling predictions with experimental data on the same polymeric materials will be reported and discussed in a forthcoming companion paper, currently under preparation.

Acknowledgements

We acknowledge the generous financial support from the Italian Ministry of University and Scientific Research (MIUR, Rome, Italy), PRIN grant “Theory, modeling and simulations for nanoscaled systems: applications to nanocomposites”. We also personally thank Prof. Jabarin for his helpful suggestions.

References

- [1] Wu G, Cuculo JA. *Polymer* 1999;40:1011–8.
- [2] Safa HL, Bourelle F. *Packag Technol Sci* 1999;12:67–74.
- [3] Rwei S-P. *Polym Eng Sci* 1999;39:2475–81.
- [4] Bang HJ, Lee JK, Lee KH. *J Polym Sci* 2000;38:2625–33.
- [5] Shi Y, Jabarin SA. *J Appl Polym Sci* 2001;81:11–22.
- [6] Patchek TD, Jabarin SA. *Polymer* 2001;42:8975–85.
- [7] Bedia EL, Murakami S, Kitade T, Kohjiya S. *Polymer* 2001;42:7299–305.
- [8] Tonelli AE. *Polymer* 2002;43:637–42.
- [9] Maruhashi Y. *Polym Eng Sci* 2003;43:169–79.
- [10] Guo M, Zachmann HG. *Polymer* 1993;34:2503–7.

- [11] Stewart ME, Cox AJ, Naylor DM. *Polymer* 1993;34:4060–7.
- [12] Okamoto M, Kotaka T. *Polymer* 1997;38:1357–61.
- [13] Ihm DW, Park SY, Chang CG, Kim YS, Lee HK. *J Polym Sci Part A Polym Chem* 1996;34:2841–50.
- [14] Kampert WG, Sauer BB. *Polymer* 2001;42:8703–14.
- [15] Kotliar AM. *J Polym Sci Macromol Rev* 1981;16:367–95.
- [16] Kimura M, Porter RS. *J Polym Sci Polym Phys Ed* 1983;21:367–78.
- [17] Porter RS, Jonza J, Kimura M, Desper C, George E. *Polym Eng Sci* 1989;29:55–62.
- [18] Andresen E, Zachmann HG. *Colloid Polym Sci* 1994;272:1352–62.
- [19] Soon KH, Lee SC, Park IH, Lee HM, Park OO, Son TW. *Polymer* 1997;38:6079–81.
- [20] Kenwright AM, Peace SK, Richards RW, Bunn A, Macdonald WA. *Polymer* 1999;40:5851–6.
- [21] Jun HW, Chae SH, Park SS, Myung HS, Im SS. *Polymer* 1999;40:1473–80.
- [22] Shi Y, Jabarin SA. *J Appl Polym Sci* 2001;80:2422–36.
- [23] Yang H, Ma J, Wengang L, Liang B. *Polym Eng Sci* 2002;42:1629–41.
- [24] Tharmapuram SR, Jabarin SA. *Adv Polym Technol* 2003;22:155–67.
- [25] Tharmapuram SR, Jabarin SA. *Adv Polym Technol* 2003;22:137–46.
- [26] Medina RM, Likhatchev D, Alexandrova L, Sánchez-Solís A, Manero O. *Polymer* 2004;45:8517–22.
- [27] Jabarin SA, personal communication.
- [28] Baltá Calleja FJ, Giri L, Zachmann HG. *J Polym Sci* 1997;32:1117–9.
- [29] Fraaije JEM. *J Chem Phys* 1993;99:9202–12.
- [30] Fraaije JGEM, van Vlimmeren BAC, Maurits NM, Postma M, Evers OA, Hoffmann C, et al. *J Chem Phys* 1997;106:4260–9.
- [31] Maurits NM, Zvelindovsky AV, Sevink GJA, van Vlimmeren BAC, Fraaije JGEM. *J Chem Phys* 1998;108:9150–4.
- [32] Altevogt P, Evers OA, Fraaije JGEM, Maurits NM, van Vlimmeren BAC. *J Mol Struct (Theochem)* 1999;463:139–43.
- [33] Sun H. *J Phys Chem B* 1998;102:7338–64.
- [34] Maple JR, Hwang MJ, Stockfisch TP, Dinur U, Waldman M, Ewig CS, et al. *J Comput Chem* 1994;15:162–82.
- [35] Hwang MJ, Stockfisch TP, Hagler AT. *J Am Chem Soc* 1994;116:2515–25.
- [36] Fermeglia M, Priol S. *AIChE J* 1999;45:2619–27.
- [37] Fermeglia M, Priol S. *Chem Eng Commun* 2003;190:1267–92.
- [38] Theodorou DN, Suter UW. *Macromolecules* 1985;18:1467–78.
- [39] Flory PJ. *Principles of polymer chemistry*. Ithaca, NY, USA: Cornell University Press; 1974.
- [40] Mattice WL, Suter UW. *Conformational theory of large molecules: the rotational isomeric state model in macromolecular systems*. New York, NY, USA: John Wiley & Sons; 1994.
- [41] Meirovitch H. *J Chem Phys* 1983;79:502–8.
- [42] Li Y, Mattice WL. *Macromolecules* 1992;25:4942–7.
- [43] Fan CF, Cagin T, Chen Z, Smith KA. *Macromolecules* 1994;27:2383–91.
- [44] Fermeglia M, Ferrone M, Priol S. *Bioorg Med Chem* 2002;10:2471–8.
- [45] Priol S, Fermeglia M, Ferrone M, Asquini A. *Carbon* 2003;41:2269–83.
- [46] Toth R, Coslanich A, Ferrone M, Fermeglia M, Priol S, Miertus S, et al. *Polymer* 2004;45:8075–83.
- [47] Berendsen HJC, Postma JPM, van Gunsteren WF, DiNola A, Haak JR. *J Chem Phys* 1984;81:3684–90.
- [48] Andersen HC. *J Chem Phys* 1980;72:2384–93.
- [49] Greengard L, Rokhlin VI. *J Comput Phys* 1987;73:325–48.
- [50] Schmidt KE, Lee MA. *J Stat Phys* 1991;63:1223–35.
- [51] Ding HQ, Karasawa N, Goddard III WA. *J Chem Phys* 1992;97:4309–15.
- [52] Verlet L. *Phys Rev* 1967;159:98–103.
- [53] de Gennes PG. *Scaling concepts in polymer physics*. Ithaca, NY, USA: Cornell University Press; 1979.
- [54] Doi M, Edwards SF. *The theory of polymer dynamics*. Oxford, UK: Clarendon Press; 1986.
- [55] Honeycutt JD. *Comput Theor Polym Sci* 1998;8:1–8.
- [56] Zhang R, Mattice WL. *Macromolecules* 1992;25:4937–41.
- [57] Zhang R, Mattice WL. *Macromolecules* 1993;26:4384–5.
- [58] Gusev AA. *J Mech Phys Solids* 1997;45:1449–59.
- [59] Gusev AA. *Macromolecules* 2001;34:3081–93.
- [60] Hiltner A, Lin RYF, Hu YS. *Boer J Polym Sci Part B* 2005;43:1047–63.
- [61] McGonigle EA, Liggat JJ, Pethrick RA, Jenkins SD, Daly JH, Hayward D. *Polymer* 2001;42:2413–26.
- [62] Van Krevelen DW. *Properties of polymers*. 3rd ed. Amsterdam, The Netherlands: Elsevier B.V.; 1990.
- [63] Mark JE. *Physical properties of polymers handbook*. Woodbury, NY: American Institute of Physics; 1997.